Interference fringe analysis using wavelet transform

Takamasa Suzuki *[a], Ryo Kiyohara [b], Mika Ichikawa [b], and Osami Sasaki[b]
[a]Niigata University, Graduate School of Science and Technology, [b]Niigata University, Faculty of Engineering, 8050 Ikarashi2, Niigata, 950-2181 Japan

ABSTRACT

Fringe analysis methods that employ wavelet transform are described. The performances of the methods are examined from the viewpoints of required calculation time and accuracy. Further, accuracies of calculations performed using linear and logarithmic scales in wavelet transform are compared. Experimental results show that wavelet signal processing is effective in measuring profiles having large and gradual asperities.

Keywords: Fringe analysis, wavelet transform, Fourier transform, instantaneous image acquisition

1. INTRODUCTION

Interferometric measurement is useful for the testing of precision components during their manufacture. A resolution of the order of a few nanometers enables the improvement of the accuracy of these precision components. However, external disturbance adversely affects the measurement accuracy of interferometers; therefore, several techniques such as feedback (FB) compensation[1] and instantaneous image acquisition[2] have been developed for maintaining the high performance of interferometers. FB compensation can easily be installed in the interferometer by making use the wavelength tunability of a laser diode (LD). This compensation, however, cannot adapt to a sudden large disturbance because of the gain-bandwidth limitation of the FB loop. Instantaneous image acquisition does not require any modification to the instrument in which it is to be introduced; it requires only one interferogram. A clear fringe pattern facilitates the calculation of the phase by eliminating disturbance. Unfortunately, instantaneous image acquisition is unsuitable for use with established analysis techniques such as phase shifting interferometry[3], sinusoidal phase modulating interferometry[4], and heterodyne interferometry[5] because these techniques require more than three images for phase extraction. In contrast, the Fourier transform (FT) method[6] can calculate the phase from just one interferogram. The FT method, however, requires a carrier fringe whose spatial frequency is constant. By this method, signal processing is carried out by focusing on a specific frequency component. The accuracy of phase calculation is restricted when the fringe exhibits a periodical pattern whose spatial frequency changes extensively over the field of view. Moreover, accurate phase calculation is difficult when the spatial frequency is high.

Recently, a frequency analysis method termed wavelet transform (WT) has attracted considerable attention in signal processing[7, 8]. This method is efficient because it can detect localized frequencies accurately and is useful for analyzing fringes[9–12] in which the spatial frequency varies extensively.

In this paper, we examine the performances of three fringe analysis methods—the FT method, a WT-based frequency analysis (WTF) method, and a WT-based phase analysis (WTP) method—that are capable of calculating the phase from a single image. We discuss and compare their performances form the viewpoints of required calculation time and accuracy. Further, the difference in accuracies achieved using WT coefficients represented by a linear-scale and a logarithmic-scale is examined. Experimental results show that WT is effective in calculating the phase from a single interferogram that contains a wide range of localized frequencies. By extracting the phase from a single interferogram (instantaneous image acquisition), we can perform disturbance-free interferometric measurements.

2. PRINCIPLE

2.1 Mathematical basis for wavelet transform

The WT of a signal $s(x)$ is defined as

*takamasa@eng.niigata-u.ac.jp; phone/fax +81-25-262-72154

2008 International Conference on Optical Instruments and Technology: Optoelectronic Measurement Technology and Applications, edited by Shenghua Ye, Guangjun Zhang, Jun Ni, Proc. of SPIE Vol. 7160
716002 · © 2009 SPIE · CCC code: 0277-786X/09/$18 · doi: 10.1117/12.817853

$$W(a,b)=\int_{-\infty}^{+\infty} s(x)\psi_{a,b}(x)dx\,, \tag{1}$$

where

$$\psi_{a,b}(x)=\frac{1}{\sqrt{a}}\psi\left(\frac{x-b}{a}\right) \tag{2}$$

is an analyzing wavelet that is obtained by the scaling and shifting of a mother wavelet $\Psi(x)$. We give interferogram as $s(x)$. Parameters a and b are termed scale parameter and shift parameter, respectively. $\Psi(x)$ is vertically magnified by $1/\sqrt{a}$ and horizontally expanded by a. The coefficient $W(a, b)$ shows the correlation strength between $s(x)$ and $\Psi_{a,b}(x)$. When a decreases, $\Psi(x/a)$ becomes narrow and has a strong correlation with the high-frequency component of $s(x)$. The local frequency f is inversely proportional to a as follows:

$$f=\frac{p}{a}\,, \tag{3}$$

where p is a proportionality constant. The parameter b indicates the position at which the analysis is carried out. By WT, the signal can be analyzed accurately by varying the abovementioned parameters.
On the other hand, the FT of $s(x)$ is defined as

$$F(\omega)=\int_{-\infty}^{+\infty} s(x)e^{-i\omega x}dx\,. \tag{4}$$

It shows the correlation strength between $s(x)$ and sinusoidal functions. An infinite and periodical signal is a prerequisite for analyzing functions using FT. Furthermore, it is difficult to identify the location where the local frequency is detected.
The configuration of the optical setup used in our analysis—a common Twyman-Green interferometer that uses an LD as a light source—is shown in Fig. 1. A reference mirror M is tilted by k so as to introduce spatial carrier frequency. To simplify the explanation, we consider a one-dimensional (1-D) interference fringe

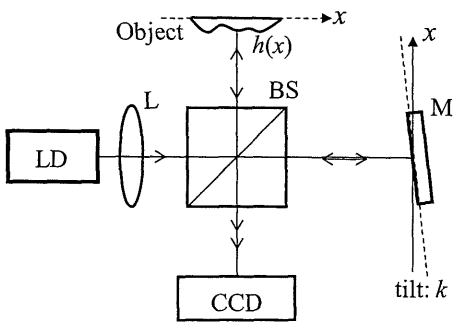

Fig. 1. Configuration of the optical setup.

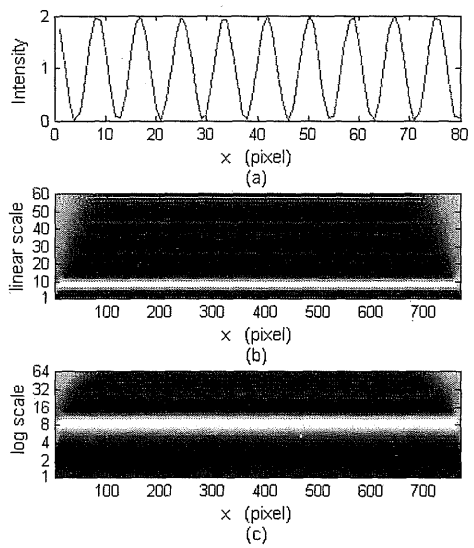

Fig. 2. Example of the wavelet coefficient obtained by WT; (a) a part of the input fringe, wavelet coefficient calculated using (b) the linear scale and (c) logarithmic scale.

$$g(x) = g_1 + g_2 \cos\alpha(x), \tag{5}$$

where g_1 is the background intensity and g_2 is the amplitude of the ac component. The phase

$$\alpha(x) = \frac{2\pi}{\lambda}[L + 2\{kx + h(x)\}] \tag{6}$$

is geometrically determined by the wavelength λ, tilt k, surface profile $h(x)$, and the optical path difference (OPD) L between the object and the mirror M. Then, Eq. (5) can be rewritten as

$$g(x) = g_1 + g_2 \cos\left[\alpha_0 + 2\pi f_0 + \frac{4\pi}{\lambda}h(x)\right], \tag{7}$$

where $\alpha_0 = 2\pi L/\lambda$ is the initial phase corresponding to the initial OPD and

$$f_0 = \frac{2k}{\lambda} \tag{8}$$

is the spatial carrier frequency determined by the tilt of M.
Figure 2 shows an example of the coefficient obtained by WT. We use the 1-D fringe as $s(x)$, whose carrier frequency is constant. A part of the fringe at $k = 80$ is shown in Fig. 2(a). When we apply WT to the fringe, wavelet coefficients are obtained as shown in Figs. 2(b) and 2(c). These coefficients are calculated using different values of a, as explained in detail later. The shading in Figs. 2(b) and 2(c) represents the intensity of $W(a, b)$. If we consider a value of a that yields the maximum intensity a_0 and substitute this a value in Eq. (3), we can determine the carrier frequency of the fringe as

$$f_0 = \frac{p}{a_0}. \tag{9}$$

From Eqs. (8) and (9), the proportionality constant p obtained at the maximum intensity a_0 is expressed as

$$p = \frac{2k}{\lambda}a_0. \tag{10}$$

2.2 Representation of WT coefficient

Parameter a used for obtaining $W(a, b)$ can be expressed by either a linear scale or a logarithmic scale. WT using the logarithmic scale enables the expansion of the analysis area within a restricted time frame. If we use a linear scale from 1 to n_1 with intervals of m_1, parameter a is represented as

$$a = 1,\ 1 + m_1, \cdots,\ n_1 - m_1,\ n_1, \tag{11}$$

and the number of data points becomes $(n_1 + m_1 - 1)/m_1$. On the other hand, if we use a logarithmic scale from $2^{\frac{1}{m_2}}$ to maximum 2^{n_2}, the parameter a is expressed as

$$a = 2^{\frac{1}{m_2}}, 2^{\frac{2}{m_2}}, \cdots, 2^{\frac{m_2(n_2-1)}{m_2}}, 2^{\frac{m_2 n_2}{m_2}}, \tag{12}$$

and the number of data points becomes $m_2 n_2$.
Examples of the wavelet coefficient calculated using the linear scale and logarithmic scale are shown in Figs. 2(b) and 2(c), respectively. The input fringe of $k = 80$, which is to be analyzed, is shown in Fig. 2(a). The wavelet coefficient calculated using a linear scale from 1 to 60 with the interval of 1 is shown in Fig. 2(b); in this case, the number of data points is 60. Because the data number is equal to a in this example, the largest coefficient is obtained at $a = 8$. Further, the wavelet coefficient calculated using the logarithmic scale with $m_2 = 10$ and $n_2 = 6$ is shown in Fig. 2(c). In this case, the maximum value of a is $2^6 = 64$ and the number of data points is $10 \times 6 = 60$. The largest wavelet coefficient is obtained at a data number of 30. Then, the value of a for the largest coefficient is $2^{(30/10)} = 8$. While the total number of

data points in the logarithmic scale is the same as that in the linear scale, the logarithmic scale enables us to expand the observation area and analyze signals in greater detail. Moreover, for the analysis of a fringe containing a wide range of spatial frequency components by using the logarithmic scale, only a small amount of data is required. In some cases, the logarithmic scale is effective in reducing the calculation time.

2.3 Fringe analysis by use of WTF and WTP

The relationship between a local frequency $f(x)$ and a phase $a(x)$ is given by

$$f(x)=\frac{1}{2\pi}\frac{d\alpha(x)}{dx}. \tag{13}$$

Substituting Eq. (6) into Eq. (13) and taking Eq. (8) into account, we obtain

$$f(x)=f_0+\frac{2}{\lambda}\frac{dh(x)}{dx}. \tag{14}$$

As $f(x)$ can be detected by WT and the carrier frequency is known, the surface profile

$$h(x)=\frac{\lambda}{2}\int\{f(x)-f_0\}dx \tag{15}$$

is calculated from the local frequency. Because no phase data is required in this method, phase unwrapping is unnecessary. This method is termed the WTF method.

If the analyzing wavelet is complex, i.e., it contains real and imaginary components, $W(a, b)$ becomes a complex number

$$W(a, b)=r+jc. \tag{16}$$

The phase is calculated by

$$\alpha(x)=\tan^{-1}\left(\frac{c}{r}\right) \tag{17}$$

at the position where $W(a, b)$ yields the maximum intensity. If $\alpha(x)$ is wrapped between zero and 2π, an unwrapping process is necessary. Then, the surface profile is given by

$$h(x)=\frac{\lambda}{2\pi}\alpha(x). \tag{18}$$

This method is termed the WTP method.

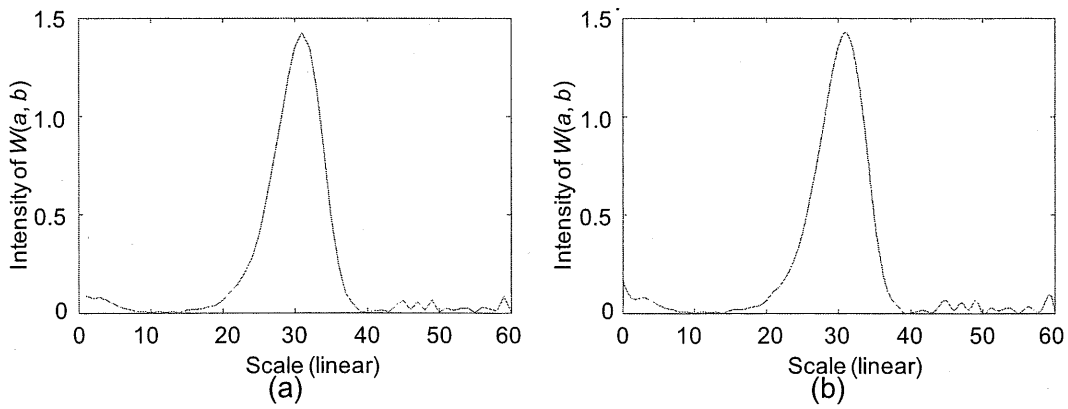

Fig. 3. Example of interpolation; (a) original $W(a, b)$ and (b) interpolated $W(a, b)$.

2.4 Interpolation of wavelet coefficient

A small step size of a is required for analyzing a fringe containing high-frequency components. However, the smaller the step size, the longer is the calculation time. Therefore, we interpolate $W(a, b)$ that has a large step size of a. We carry out cubic spline interpolation and polynomial fitting. An example of cubic spline interpolation carried out on the linear scale with $m_1 = 1$ is shown in Fig. 3. The original coefficient $W(a, b)$ along the x-axis is shown in Fig. 3(a). Although we can observe a peak in Fig. 3(a), it is not accurate because the interval at which data is obtained is an integer. The interpolated $W(a, b)$, shown in Fig. 3(b), is smooth and yields the best estimate of the phase.

3. COMPARISON OF THE PERFORMANCES IN THREE METHODS

By performing numerical calculations, we examine the phase extraction performances of the three methods. The mother wavelet used in our analysis is the complex Morlet wavelet

$$\psi(x)=\frac{1}{\sqrt{\pi}}\exp(2\pi ix)\exp\left(-x^2\right). \tag{19}$$

Because this wavelet consists of real and imaginary components, it facilitates the extraction of phase distribution from the interferogram. We use a CCD camera for instantaneous image acquisition and assume its pixel size to be 10 μm and the wavelength of light to be 655 nm, which are standard values for this device. To simplify the analysis, we use a 1-D profile as an object.

3.1 Examples of calculations

Examples of calculations at $k = 80$ are shown in Figs. 4, 5, and 6. We assumed a Gaussian shape with a maximum height of 100 nm for an input. Cubic spline interpolation was carried out in the WTF method. Steps involved in signal processing based on the WTF method are shown in Fig. 4. This calculation was performed using the logarithmic scale with $m_2 = 10$ and $n_2 = 6$. We (a) determined the surface profile and (b) generated the interference fringe as shown in Fig. 4. From (c) the wavelet coefficient $W(a, b)$ calculated using the logarithmic scale, we (d) determined the maximum value of $W(a, b)$ at each position and (e) converted it to the local frequency $f(x)$. After (f) removing the carrier frequency, we (g) obtained the phase distribution and (h) surface profile by using Eq. (15).

Another example of steps involved in fringe analysis based on the WTP method is shown in Fig. 5. The analysis was carried out using the linear scale with $m_1 = 1$ and $n_1 = 60$. Figures 5(a) and 5(b) are identical to Figs. 4(a) and 4(b). In this analysis, (c) the intensity of $W(a, b)$ and (d) its phase were calculated using the linear scale. As (e) the phase at the maximum value of $W(a, b)$ was wrapped within 0 and 2π, we (f) calculated the unwrapped phase and (g) eliminated the tilt. Finally, we (h) obtained the surface profile using Eq. (18).

Figure 6 shows the steps involved in the calculation based on the FT method. From (c) the frequency components obtained by fast Fourier transform (FFT), we (d) selected the frequency component of the spatial carrier (e) eliminated the carrier frequency component, (f) shifted them to the both edges of x-axis so as to calculate inverse-FFT, and (g) obtained the phase distribution. Then, (h) the profile was calculated by using Eq. (18).

3.2 Dependence of accuracy on the spatial frequency

We examined accuracies corresponding to the spatial carrier frequency. Because the carrier frequency changes with k, we varied k from 30 to 80 with the interval of 2. These values correspond to spatial frequencies in the range of 90 to 240 (1/μm). We estimated errors in the methods by using the standard deviation

$$D=\sqrt{\frac{\sum_{j=1}^{N}\left\{h_1(j)-h_2(j)\right\}^2}{N}}, \tag{20}$$

where h_1 and h_2 are the given and calculated profiles, respectively, and N is the total data number. For the WTF method, the error due to the increase in the carrier frequency is calculated as shown in Fig. 7. Over the entire range of spatial frequencies, the error calculated by the logarithmic scale is smaller than that by the linear scale; however, there are no significant differences between the accuracies obtained using the two scales. Figure 8 shows the variation in the error in the WTP method with the increase in the carrier frequency. In this case, the error in the carrier frequency obtained using the linear scale is small.

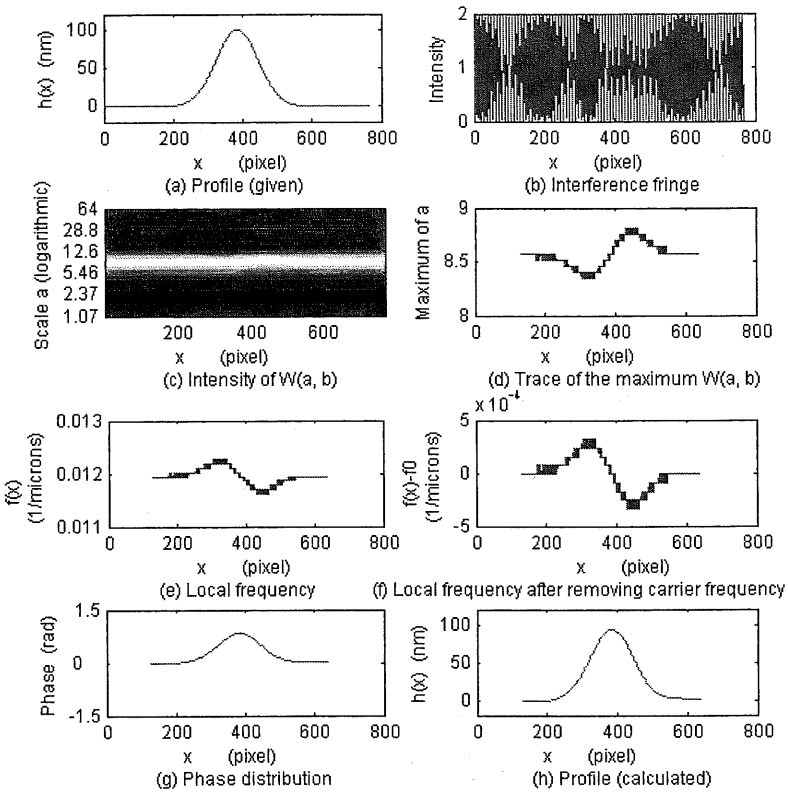

Fig. 4. Steps involved in signal processing based on the WTF method using the logarithmic scale with $m_2 = 10$ and $n_2 = 6$.

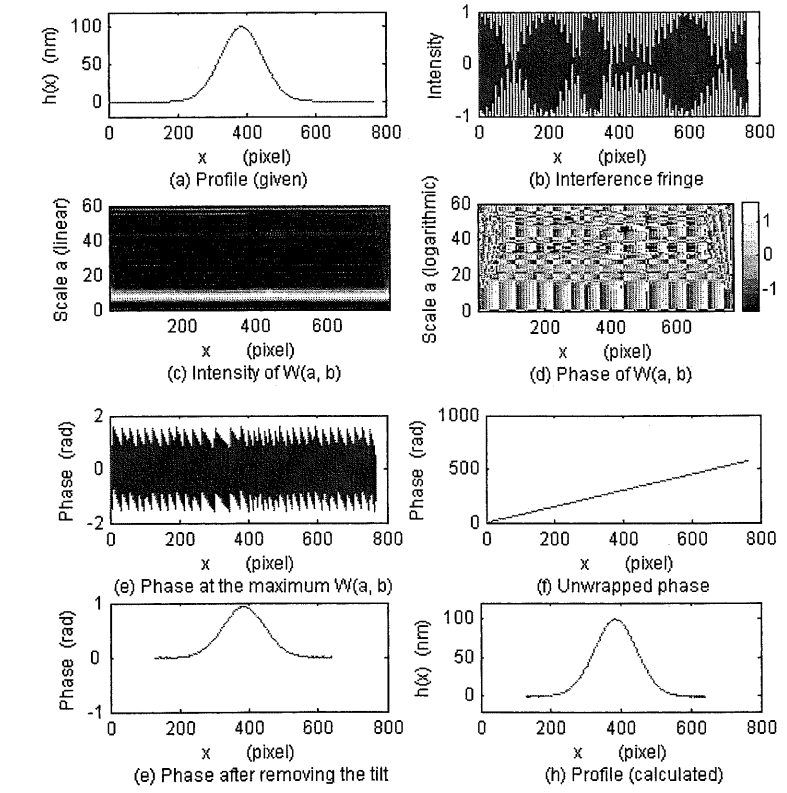

Fig. 5. Steps involved in signal processing based on the WTP method using the linear scale with $m_1 = 1$ and $n_1 = 60$.

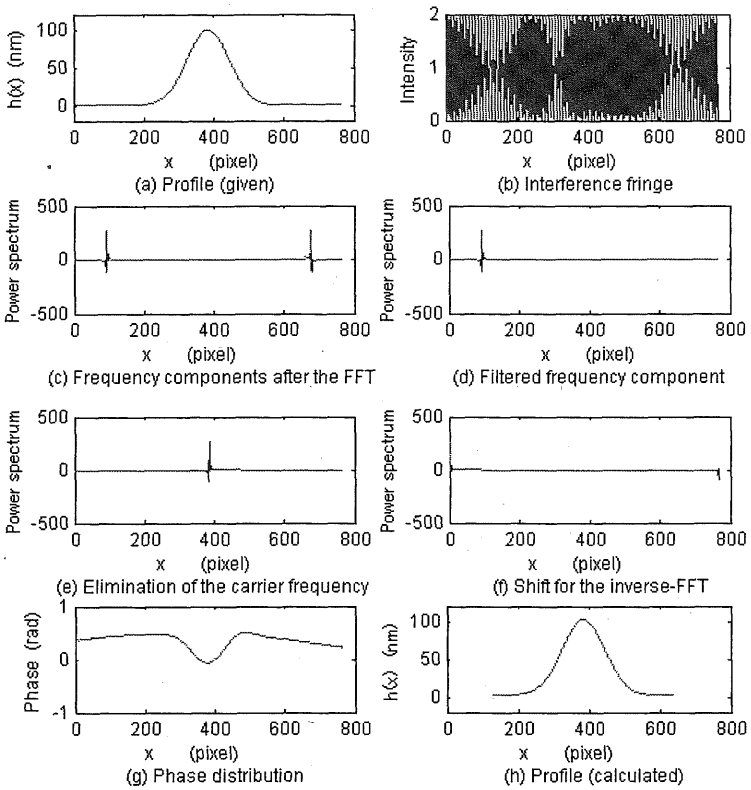

Fig. 6. Steps involved in signal processing based on the FT method.

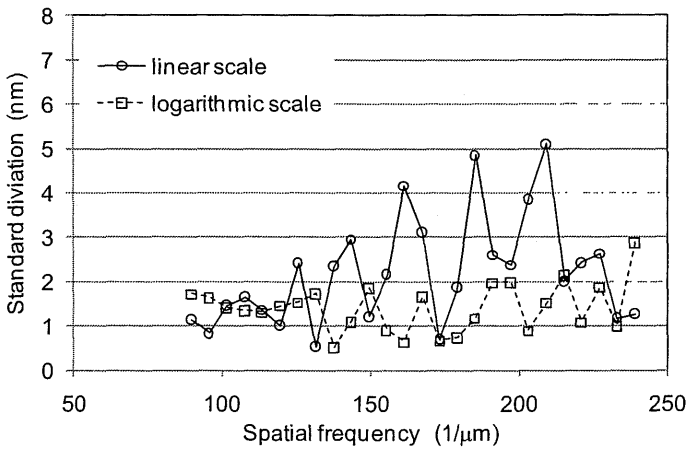

Fig. 7. Error due to the increase in the carrier frequency in the WTF method.

We performed similar calculations for the FT method so as to compare its performance with that of WT. The calculation results show that the error is not very large over the entire range of carrier frequencies; however, the change in frequency affects the accuracy of the methods, as shown in Fig. 9. The amplitude of error variation shown in Fig. 9 is larger than those shown in Figs. 7 and 8.

3.3 Dependence of accuracy on object shape

The local frequency varies with not only the tilt but also the shape of the object. We investigated the change in accuracy with the object shape. Figure 10 shows the comparison between the given and calculated profiles. We brought Figs. 4(h),

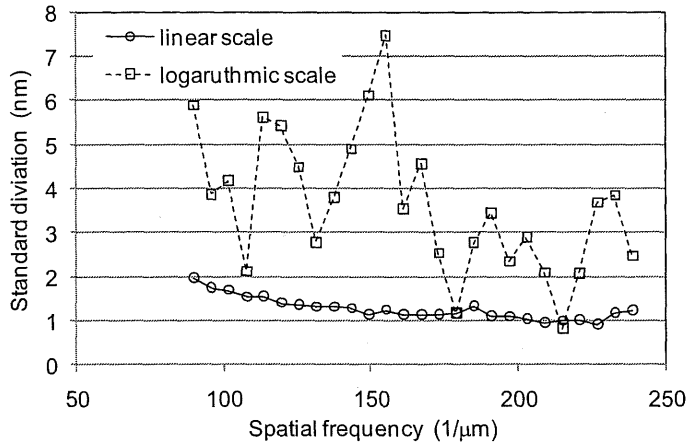

Fig. 8. Error due to the increase in the carrier frequency in the WTP method.

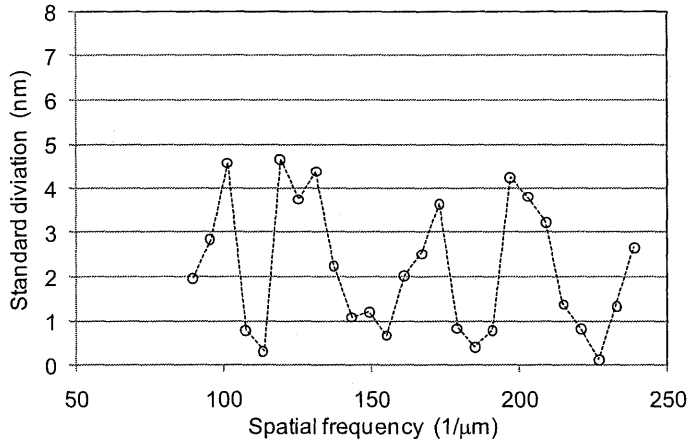

Fig. 9. Error due to the increase in the carrier frequency in the FT method.

5(h), and 6(h) together in Fig. 10. Calculation times and the errors estimated using the standard deviation are shown in Table 1. Because the cubic spline interpolation was carried out in the WTF method (Fig. 4), the calculation required a long time. The results show that the performance of the WTP method is the best.

Calculations for another profile are shown in Fig. 11. Conditions under which WT was carried out were the same as those of the WTF method, whose results are shown in Fig.10. When a rectangular shape with a height of 100 nm was used as shown in Fig. 11(a), calculation results obtained by the WTF, WTP, and FT methods were shown in Figs. 11(b), 11(c), and 11(d), respectively. The estimation errors and times required for calculations are shown in Table 2. While the performance of the WTP method is considerably better than that of the WTF method, it is slightly inferior to the performance of the FT method.

3.4 Dependence of accuracy on interpolation

Figure 11 (b) shows that interpolation is necessary in the WTF method. We examined the effect of interpolation on the accuracy of the WT method by performing calculations. In these calculations, we used a linear scale with $m_1 = 0.1$ and $n_1 = 16$. Calculation results obtained by the WTF method are shown in Fig. 12. The input shape was rectangular with a height of 100 nm, as shown in Fig. 12(a). When interpolation was not carried out, the rectangular shape changed slightly as shown in Fig. 12(b), and some noise was observed. When the cubic spline interpolation was carried out, the noise decreased and the shape became as shown in Fig. 12(c). Figure 12(d) shows the result obtained by the WTF method, in which polynomial fitting was carried out. No significant noise is observed in the profile shown in Fig. 12(d).

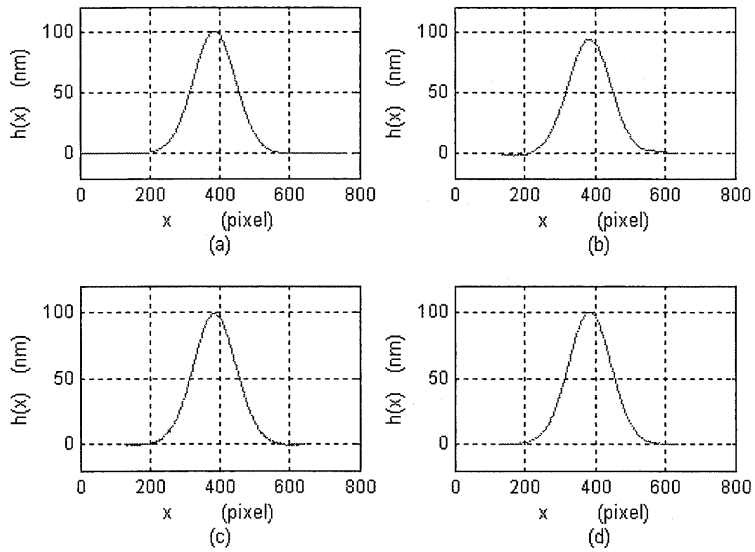

Fig. 10. Comparison between (a) the original Gaussian profile and calculation results obtained by (b) the WTF, (c) WTP, and (d) FT methods.

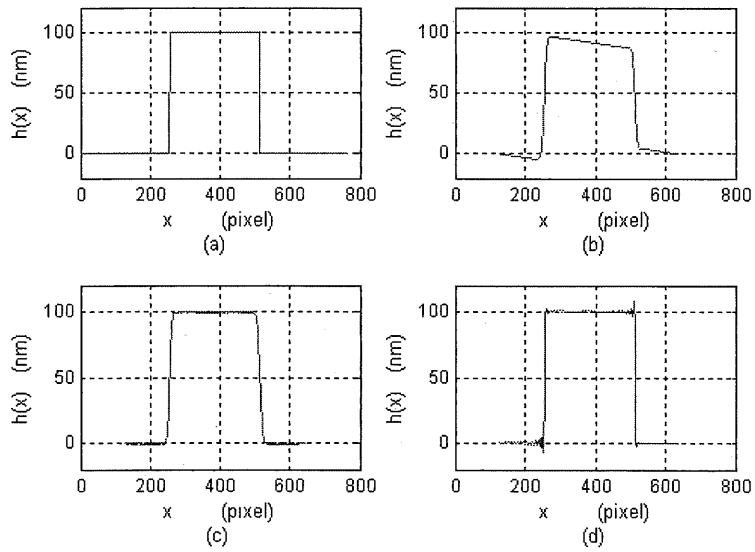

Fig. 11. Comparison between (a) the original rectangular profile and calculation results obtained by (b) the WTF, (c) WTP, and (d) FT methods.

Table 1. Calculation times and the errors in Fig. 10.

	WTF	WTP	FT
error (nm)	2.88	0.59	2.28
time (sec)	4.32	1.12	0.57

Table 2. Calculation times and the errors in Fig. 11.

	WTF	WTP	FT
error (nm)	9.91	7.38	4.15
time (sec)	4.14	1.35	0.59

The estimated errors and the calculation times for the results shown in Fig. 12 are listed in Table 3. Although the time required for calculation increases as the complexity of the fitting process increases, the performance of the WTF method improves.

The calculation results of the WTP method are shown in Fig. 13. The original profile is shown in Fig. 13(a). Results obtained without interpolation, with the cubic spline interpolation, and with the polynomial fitting are shown in Figs. 13(b), 13(c), and 13(d), respectively. From these results, we observe that these three interpolation methods yield almost the same profile. Table 4 shows the calculation times and estimated errors. From Table 4, we can observe that the accuracy does not significantly depend on the interpolation method. The calculation times, however, differ according to the interpolation method. From Fig. 13(b), we can observe that no interpolation is necessary in the WTP method.

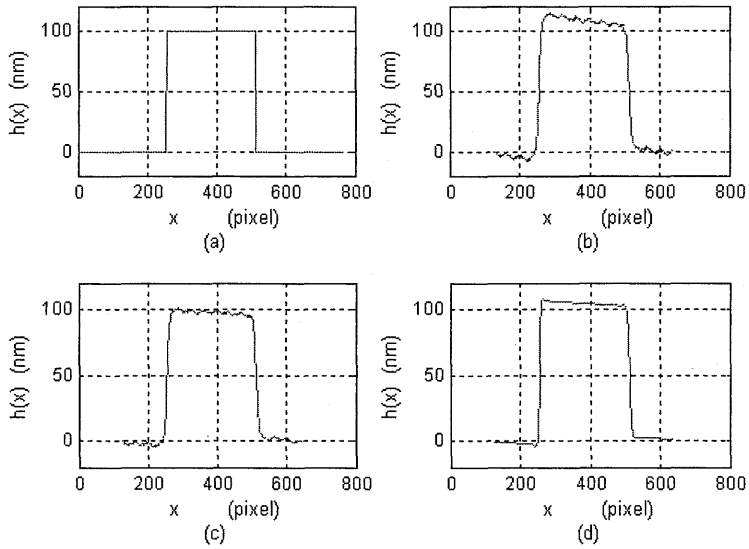

Fig. 12. Calculation results obtained by the WTF method; (a) the original rectangular profile and results obtained (b) without an interpolation, (c) with a cubic spline interpolation, and (d) with a polynomial fitting.

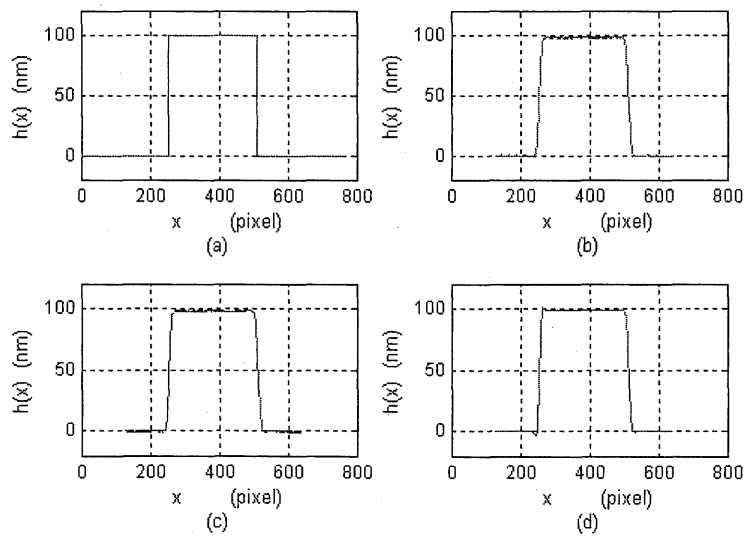

Fig. 13. Calculation results obtained by the WTP method; (a) the original rectangular profile and results obtained (b) without an interpolation, (c) with a cubic spline interpolation, and (d) with a polynomial fitting.

Table 3. Calculation times and the errors in Fig. 12.

	none	spline	polynomial
error (nm)	9.60	7.94	6.77
time (sec)	0.43	0.69	1.99

Table 4. Calculation times and the errors in Fig. 13.

	none	spline	polynomial
error (nm)	7.59	7.61	6.95
time (sec)	0.37	0.49	3.63

4. EXPERIMENTS

We performed some experiments using the setup shown in Fig. 1. The central wavelength and power of the LD were 655 nm and 5 mW, respectively. A concave mirror whose radius of curvature (ROC) was 2500 mm was used as the object. A series of experimental process are shown in Fig. 14. The observed interference fringe at k = 0 is shown in Fig. 14(a), within which many fringes are observed. Because the mirror has a large ROC, it is difficult to introduce a carrier fringe into the original fringe. When the FFT is applied, for instance, to the interference fringe shown in Fig. 14(a), no discriminative frequency components are detected, as shown in Fig. 15. That is, such an image that originally contains many fringes cannot be analyzed by the FT method.

On the other hand, when the WTP method was applied to the fringe shown Fig. 14(a), distributions of the intensity and phase of W(a, b) were obtained as shown in Figs. 14(b) and 14(c), respectively, and even the surface profile is detected accurately, as shown in Fig. 14(d).

5. CONCLUSIONS

We evaluated three types of signal processing methods capable of analyzing a single interference fringe accurately. After establishing the theoretical accuracies of the methods the performance of WT for fringe analysis was examined in contradistinction to that of the FT method. Parameter a used for obtaining $W(a, b)$ can be expressed by either a linear scale or a logarithmic scale. WT using the logarithmic scale enables the expansion of the analysis area within a restricted time frame. However, the accuracy of WT depends to a small extent on the spatial carrier frequency. Although the WTF method does not require phase unwrapping because it uses local frequencies, it is difficult to improve the accuracy of this method without carrying out an appropriate interpolation. The WTP method does not require interpolation and its accuracy is higher than those of the WTF method and FT method when the object has no sudden changes in the profile. It is concluded that the performance of the WTP method for analyzing a single interferogram is good in terms of the method's accuracy and required calculation time.

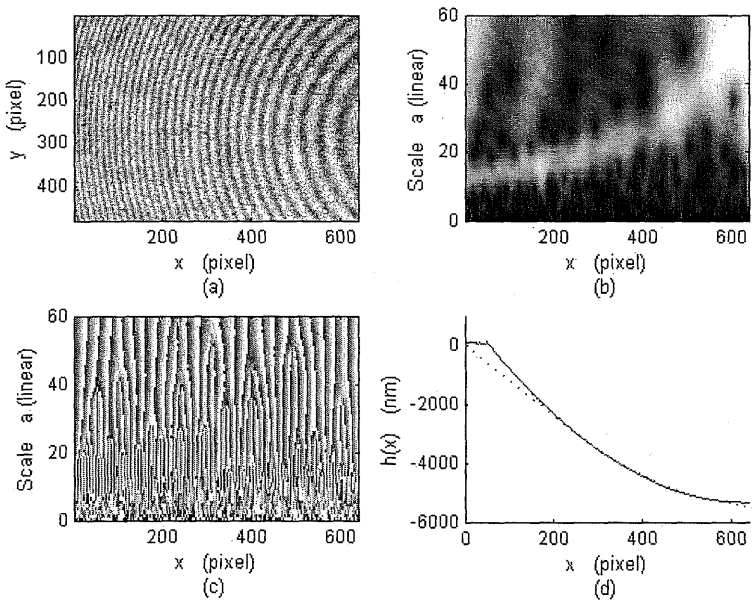

Fig. 14. A series of experimental process. (a) the observed interference fringe at k = 0, distribution of (b) the intensity and (c) phase of W(a, b) calculated with the WTP method, (d) detected profile.

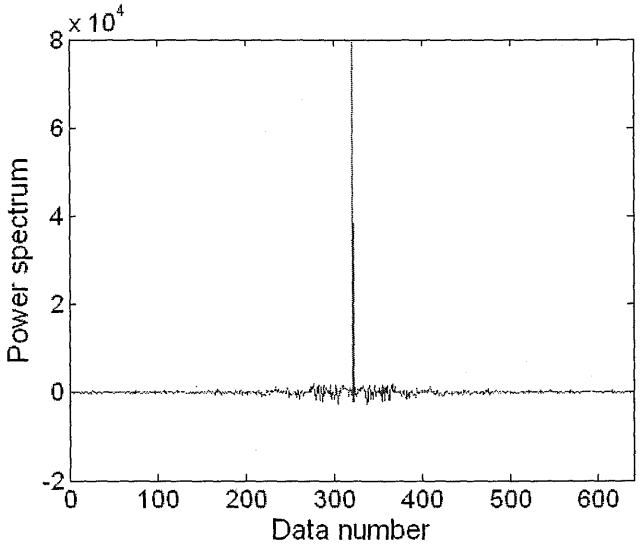

Fig. 15. Frequency analysis of the interference fringe shown in Fig. 14(a).
No discriminative frequency components are detected with the FFT.

REFERENCES

[1] O. Sasaki, K. Takahashi, and T. Suzuki, "Sinusoidal phase modulating laser diode interferometer with a feedback control system to eliminate external disturbance," Opt. Eng. **29**(12), 1511-1515 (1990).

[2] T. Suzuki, M. Ohida, K. Yokoyama, and O. Sasaki, "Stroboscopic two-wavelength interferometer for disturbance-free step-height measurement," Proc. of the 89th OSA annual meeting on CD-ROM, **JTuC7** (2005).

[3] J. E. Greivenkamp and J. H. Bruning, "Phase shifting interferometry," in *Optical Shop Testing*, Second Edition, D. Malacara, ed., pp.515-518, Wiley, New York (1992).

[4] O. Sasaki and H. Okazaki, "Sinusoidal phase modulating interferometry for surface profile measurement." Appl. Opt. 25(18), 3137-3140 (1986).

[5] K. Tatsuno and Y. Tsunoda, "Diode-laser direct modulation heterodyne interferometer," Appl. Opt. 26(1), 37-40 (1987).

[6] M. Takeda, H. Ina, and S. Kobayashi, "Fourier-transform method of fringe-pattern analysis for computer based topography and interferometry," J. Opt. Soc. Am., 72(1), 156-160 (1982).

[7] H. L. Resnikoff, "Wavelet and adaptive signal processing," Opt. Eng. 31(6), 1229-1234 (1992).

[8] A. D. McAulay, J. Wang, and J. Li, "Optical wavelet transform classifier with positive real Fourier transform wavelets," Opt. Eng. 32(6), 1333-1339 (1993).

[9] L. R. Watkins, S. M. Tan, and T. H. Barnes, "Determination of interferometer phase distributions by use of wavelets," Opt. Lett.**24**, 905-907 (1999).

[10] C. A. Sciammarella and T. Kim, "Determination of strains from fringe patterns using space-frequency representations," Opt. Eng. 42(11), 3182-3193 (2003).

[11] Z. Wang, "Advanced continuous wavelet transform algorithm for digital interferogram analysis and processing," Opt. Eng. 45(4), 045601 (2006).

[12] S. Zheng, W. Chen, and x. Su, "Adaptive windowed Fourier transform in 3-D shape measurement," Opt. Eng. 45(6), 063601 (2006).